SSIM 2021 - PM Dight (ed.)

doi:10.36487/ACG_repo/2135_20

# Compaction faulting in thick mudstone: a slope stability case study of Prominent Hill open pit mine, South Australia

**MJ Fowler** *PSM, Australia*

**DJ Goodchild** *OZ Minerals Ltd, Australia*

## Abstract

*This case study presents the conditions and performance of a sequence of weak sedimentary rocks at the OZ Minerals Ltd, Prominent Hill open pit mine located in South Australia. The weak rocks form a 100 m thick barren horizontally bedded cover sequence of Permian and Cretaceous age that overlie the ore-bearing Archaean to Mesoproterozoic basement rocks.*

*Mining of the cover sequence rocks occurred in several stages between 2006 and 2012, during which a significant number of large-scale slope instabilities occurred. The failures occurred due to a unique set of geotechnical conditions. All slope instabilities were structurally bound by polygonal faults; a type of compaction discontinuity that occurs in thick, weak, saturated mudstone sequences.*

*We highlight the origin and nature of polygonal faults and implication for slope stability and the engineering geology, geotechnical properties, pore pressure conditions, operational risk management, and design approaches including back and forward analysis.*

*Comprehensive geotechnical monitoring and risk management was successfully employed to maintain safe mining operations. The slope instabilities proved manageable in part due to the long delay between excavation and collapse. A range of operational approaches to managing the instabilities were undertaken including unloading, buttressing, and managed collapse.*

**Keywords:** *mine slope stability, weak rocks, compaction faulting, polygonal faulting, hydromechanical coupling, Bulldog Shale, Prominent Hill*

## 1 Introduction

This case study presents the conditions and performance of weak sedimentary rocks at the OZ Minerals Ltd, Prominent Hill open pit mine located in South Australia. The location of the project is shown in Figure 1. Mining of the cover sequence and the slope instabilities that are documented here occurred in excess of a decade ago. The analyses presented in this paper reflect the cost-effective technology readily available at the time.

More importantly, the key objective of the case study is to highlight the occurrence of polygonal faulting; a type of compaction discontinuity that occurs in thick, weak, saturated mudstone sequences (Cartwright & Dewhurst 1998).

The interaction of moderately steep polygonal faulting, weak substance strength (less than 10 MPa), high pore pressures, and bedding anisotropy resulted in significant but manageable wall failures.

This paper presents the engineering geology, geotechnical properties, pore pressure conditions, operational risk management, and design approaches including back and forward analysis of failures in the cover sequence rocks. For reference, field estimated strength referred to in this paper uses the PSM classification (Duran 2014).

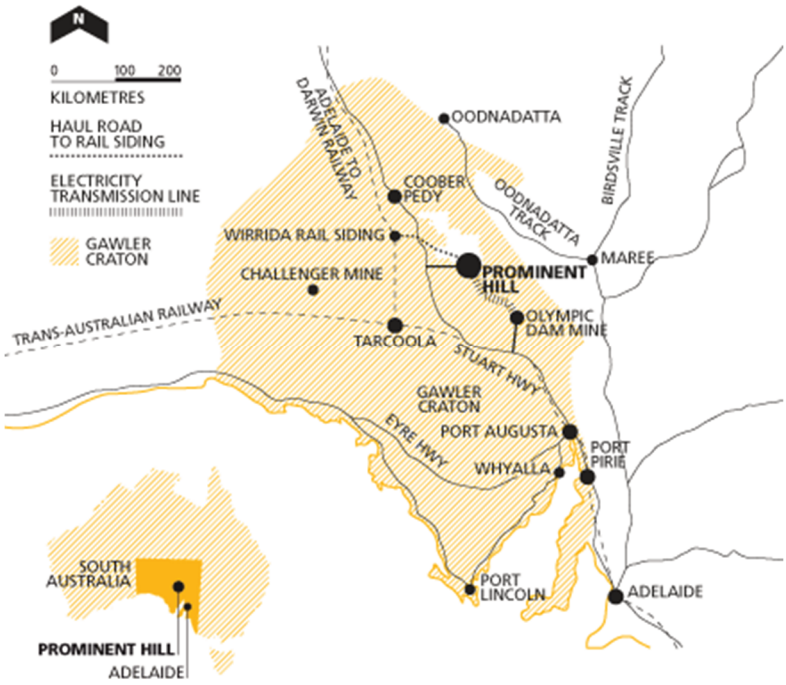


**Figure 1 Prominent Hill location plan (OZ Minerals Ltd 2009)**

# 2 Background

## 2.1 Overview

The Prominent Hill mine is located some 130 km southeast of the town of Coober Pedy and 130 km northwest of BHP's Olympic Dam mine.

The Prominent Hill deposit, located at the northern edge of the Gawler Craton, is an iron oxide copper–gold deposit, similar to Olympic Dam. The focus of this case study is the 100 m of weakly consolidated sedimentary cover which overlies the Prominent Hill deposit.

The copper–gold mineralisation has been defined across a 1,000 m strike length and to a depth of 500 m, hosted in a large hematite breccia complex. The orebody is open to both the east and west, and at depth. The central section of the orebody is the target of open pit mining while the extensions are being targeted using underground methods. Copper mineralisation within the breccia changes from a higher-grade chalcocite dominant assemblage in the upper part of the orebody, through a bornite-chalcopyrite transition zone, into chalcopyrite dominant assemblage in the lower part of the orebody. Gold is co-incident with the copper and as gold-only zones.

The orebody was discovered in 2001, first mining commenced in October 2006, and first ore production occurred in February 2009. The open pit mine ceased operations in 2018 and underground mining of the resource continues today. The mine produces copper–gold concentrate from an open pit, and processes it through a conventional crushing, grinding, and flotation circuit. On completion, the open pit is approximately 500 m deep, 1.4 km wide and 1.6 km long.

## 2.2 Cover sequence geology

The cover sequence comprises horizontally bedded low strength sedimentary rocks and soils of Permian and Cretaceous age that blanket the area. These sediments are primarily mudstones and shales, and to a lesser extent, sandstones and diamictites of the overlapping Arckaringa (Permian) and Eromanga (Cretaceous) basins as shown in Figure 2.

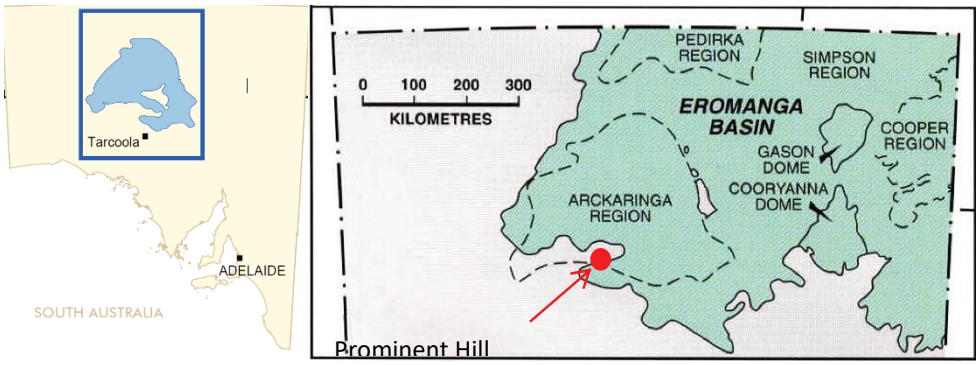


**Figure 2 Plan showing the overlapping Arckaringa and Eromanga sedimentary basins (Geological Survey of South Australia 1993)**

The pit exposure of these sediments is an approximately 100 m thick sequence and comprises:

- Variably weathered Bulldog Shale of approximately 70 m thick.
- Underlain by the Cadna-owie Sand with variable cementation, approximately 15 m thick.
- Underlain by mudstone and diamictite of another 15 m thickness on average, but this unit varies in thickness from 0–60 m.

### *2.2.1 Eromanga Basin (Jurassic–Cretaceous sediments)*

The upper and major portion of the cover sequence rocks at the Prominent Hill deposit comprises Cretaceous age marginal marine to marine sediments of the Eromanga Basin. The Eromanga Basin unconformably overlies the Arckaringa Basin (Figure 2).

The basin is a succession of sandstone and mudstone units thought to reflect an oscillating sea level. The period was dominated by a marginal marine depositional environment which later became marine transgressive up-sequence in the early Cretaceous.

The main units encountered at Prominent Hill are the Bulldog Shale of the Marree Subgroup, and the Cadna-owie Formation (referred to as Cadna-owie Sands). Details of these two units are set out in Sections 2.2.1.1 and 2.2.1.2.

#### *2.2.1.1 Bulldog Shale*

The Bulldog Shale is a grey marine mudstone. Its maximum thickness is 340 m in the northeast and thins to the west. At Prominent Hill, the thickness is less than 80 m. Outcropping Bulldog Shale has commonly undergone chemical alteration by weathering events.

The Bulldog Shale consists of dark grey bioturbated and fossiliferous shaly mudstone, with fine-grained sand intervals. Carbonaceous matter and pyrite are also present within the unweathered sections. An organic-rich dark shale forms the basal 10–25 m of the unit.

In marginal areas, the basal portion of the Bulldog Shale contains lonestones up to very large boulder size and abundant fossilised wood. The middle of the unit contains ellipsoidal limestone concretions 1 m thick and 2–3 m across. The upper section contains a higher percentage of fine sand and fossil assemblages dominated by bivalves.

The Bulldog Shale is a shelf mud deposited from suspension in the epicontinental sea. Oxygen-poor or restricted marine conditions prevailed in the early transgressive stage as represented by the basal dark organic shale with very low diversity of fossils.

As the sea advanced, conditions changed to an oxygenated marine environment as indicated by the abundance of macrofossils. Sandy layers along the western margin represent storm-related deposits.

#### *2.2.1.2 Cadna-owie Formation*

The Cadna-owie Formation is a thin, fine-grained sand unit that extends through the Eromanga Basin. It is the result of the transition from terrestrial-freshwater to marine deposits. The unit is typically 10–20 m thick at the basin margins, and up to 100 m thick in the deeper parts of the basin. The upper boundary is sharp, marked by a sudden change from calcareous sandstone to mudstone.

The Cadna-owie Formation comprises:

- Pale grey siltstone and very fine to fine-grained sandstone with laterally extensive or locally developed medium to coarse-grained sandstone interbeds.
- Locally occurring pebbly, layered diamictites and coarse, sedimentary breccia.
- Large, rounded lonestones up to boulder size widely distributed around the margin. The stones mainly consist of quartzite, igneous or gneissic lithologies.
- Sand comprised predominantly of quartz with lesser amounts of mica, fresh feldspar, heavy minerals, pyrite and glauconite.
- Cementation of sands by coarse calcite crystals, ferruginisation and carbonate.

Sedimentary structures that are observed in the Cadna-owie include:

- Upward coarsening.
- Thick bedding.
- Predominantly parallel bedding with minor cross-bedding.

The Cadna-owie Formation is interpreted to be deposited in the coastal regions of the early Cretaceous sea and represents a variety of marginal marine to non-marine environments including:

- Near offshore or outer shore.
- Inner shoreface to shoreface.
- Shallow, agitated waters of marine shoal or lagoonal shoreline.
- Intertidal zones.
- High-gradient beaches.
- Back barrier lagoon or coastal marshes.
- Fluvial environments.

### *2.2.2 Arckaringa Basin (Permian sediments)*

The lower portion of the cover sequence rocks comprises Permian age sediments of the Boorthanna and the Stuart Range Formation. The Arckaringa Basin is shown in Figure 2. The Boorthanna Formation is a glacigene sequence and the Stuart Range Formation represents marine facies towards the top. There are typically two units:

- Diamictite with shale intercalations (Boorthana Formation): The basal unit is sandy to bouldery claystone, which is often calcareous, inter-bedded with shale and occasionally thin sandstone or carbonate. It is interpreted that this unit was sub-aqueously redeposited glacial debris transported downslope as mud flows.
- Homogeneous marine shale (Stuart Range Formation): Overlying the diamictite, this unit comprises marine shale with minor siltstone and sandstone. It is interpreted to be deposited in quiet marine conditions.

## 2.3 Cover sequence faulting

The understanding of faulting in the cover sequence evolved throughout the investigation and mining phases. During the investigation phase, faults were identified in diamond drill cored holes as very widely spaced slickensided defects, although the stratigraphy correlated horizontally suggested that no major offsets existed. Early exposures identified the extent of faulting, and research of similar environments identified the polygonal faulting regime. The following section provides a regional overview and description of the genesis of polygonal faulting.

### *2.3.1 Regional seismic interpretation*

Polygonal-style faulting was identified in 3D seismic petroleum exploration at Lake Hope (Figure 3) some 360 km northeast of Prominent Hill in the same stratigraphy. The seismic survey identified steep faults with variable strike length and spacing ranging from a minimum of 100 m to an average of about 1 km. The plan of faulting shows the variable strike of the faults with some polygonal-shaped cells, as well as linear and random distributions.

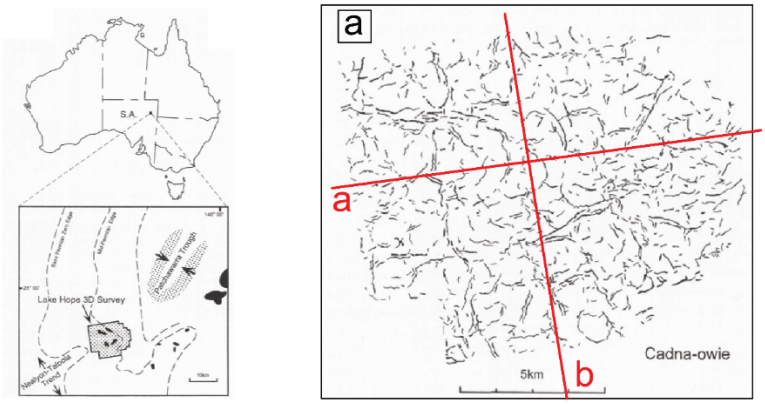


**Figure 3 (a) Location of 3D seismic survey at Lake Hope; (b) Plan of fault interpretation with cross-section locations shown in Figure 4 (Watterson et al. 2000)**

In sections, the faults are moderately steep and continuous through the Bulldog Shale and the overlying mud rocks, but do not penetrate the Cadna-owie Sands below as presented in Figure 4.

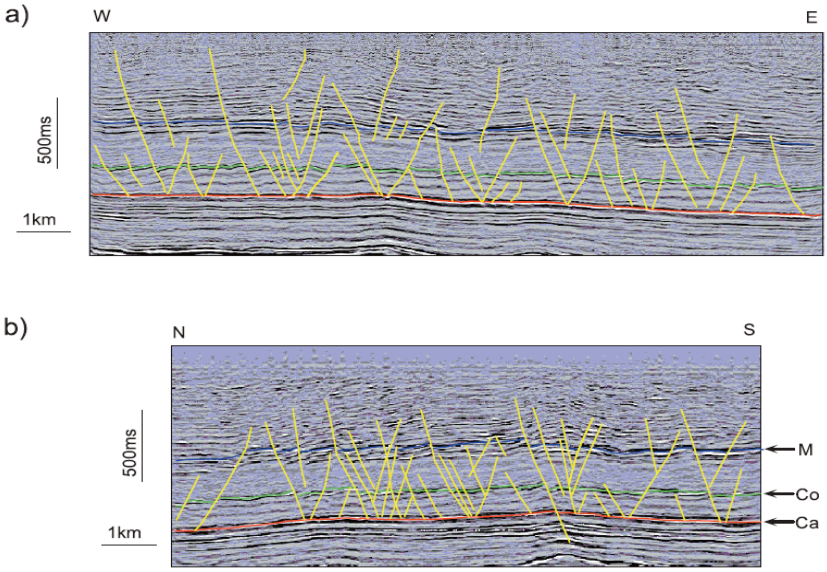


**Figure 4 Cross-sections (a) and (b) through the Lake Hope seismic interpretations showing interpreted polygonal faults in yellow terminating (with the exception of one instance) at the red line which represents the Cadna-owie Sands (Ca) (after Watterson et al. 2000)**

The results of the seismic survey are a good match with observations of exposures at the mine. One difference is that spacing of faults from the seismic survey is much wider (100–1,000 m) than that experienced onsite (~50 m). An explanation for this is that seismic profiling has difficulty identifying small displacement faults and there is an abundance of these in the outcrop.

### *2.3.2 Polygonal faulting mechanism*

The term 'polygonal' faulting is derived from the plan shape faulted cells that occur similar in plan to desiccation cracking in clayey soil although at very different scales. Polygonal faulting has been the subject of detailed investigation in petroleum exploration of the North Sea where similar lithologies are encountered.

The precise mechanism for this type of faulting is still a matter of some conjecture. The features that are common to the different theories are:

- Faulting is not tectonically related.
- It occurs in very low permeability and low strength rocks.
- Where materials are saturated and pore pressures increase due to overburden.
- Faults are probably associated with volumetric contraction due to compactional dewatering during lithogenesis.

This concept is shown diagrammatically in Figure 5 which shows two slightly different pore pressure related mechanisms (Cartwright & Dewhurst 1998). The first of these appears the best fit for the evidence at Prominent Hill based on observations of marker units exposed in the pit.

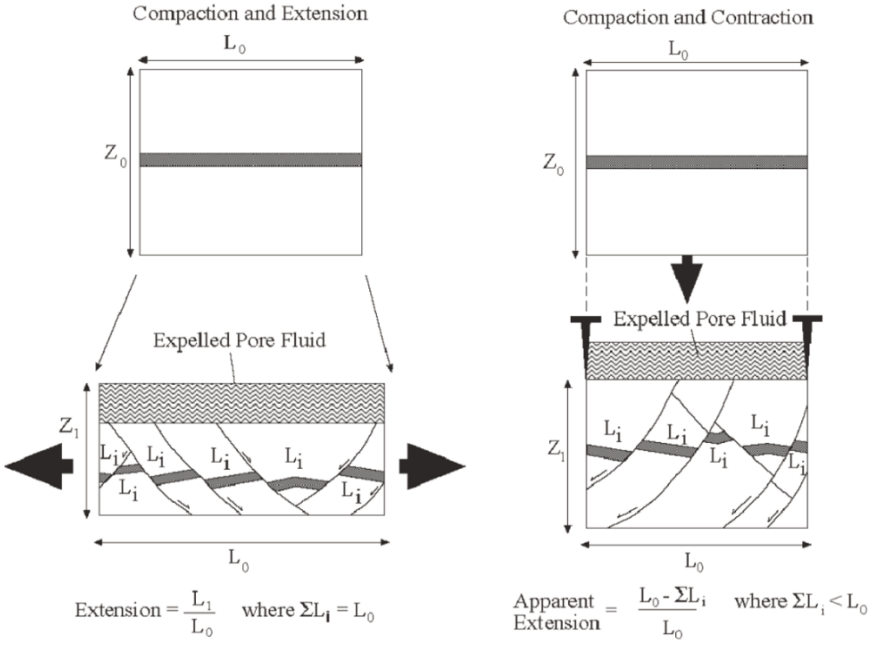


**Figure 5 Fault genesis after Cartwright & Dewhurst (1998). Two alternative strain paths are illustrated: (a) Compaction in an extensional environment; (b) Compaction with lateral confinement**

# 3 Engineering geology

## 3.1 Engineering subdivision of the cover sequence

The engineering subdivision of the cover sequence materials is presented in cross-section in Figure 6 with an overview of excavated slopes shown in Figure 7. The subdivision of the cover sequence is based on stratigraphy as described previously in Section 2.2, and weathering. The Bulldog Shale is subdivided into silcrete, oxidised Bulldog Shale, clay oxidised Bulldog Shale, and fresh Bulldog Shale.

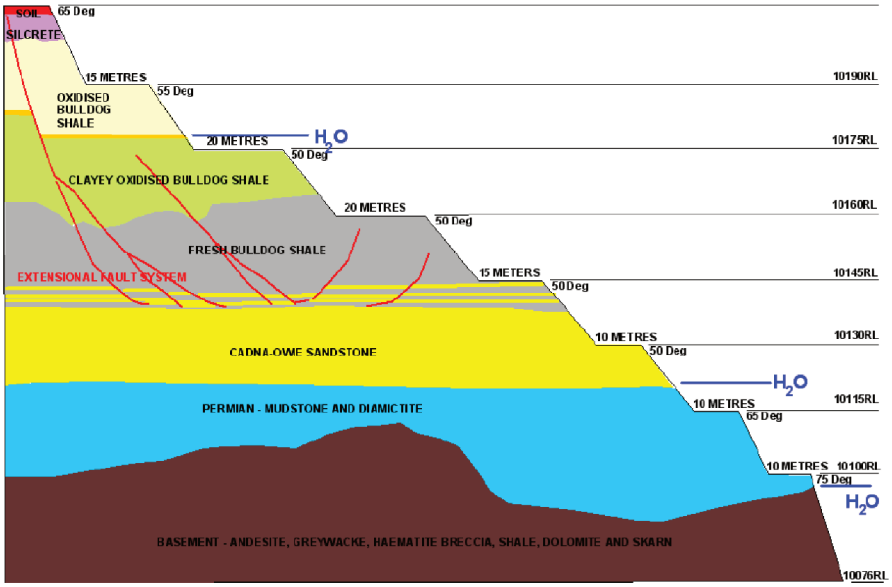


**Figure 6 Cross-section through a typical mine slope showing the engineering subdivision of the sedimentary units. The red lines represent the polygonal faults which are the focus of the paper. The typical slope geometry is annotated on each bench. $H_2O$ represents the locations of visible seepage on the pit face**

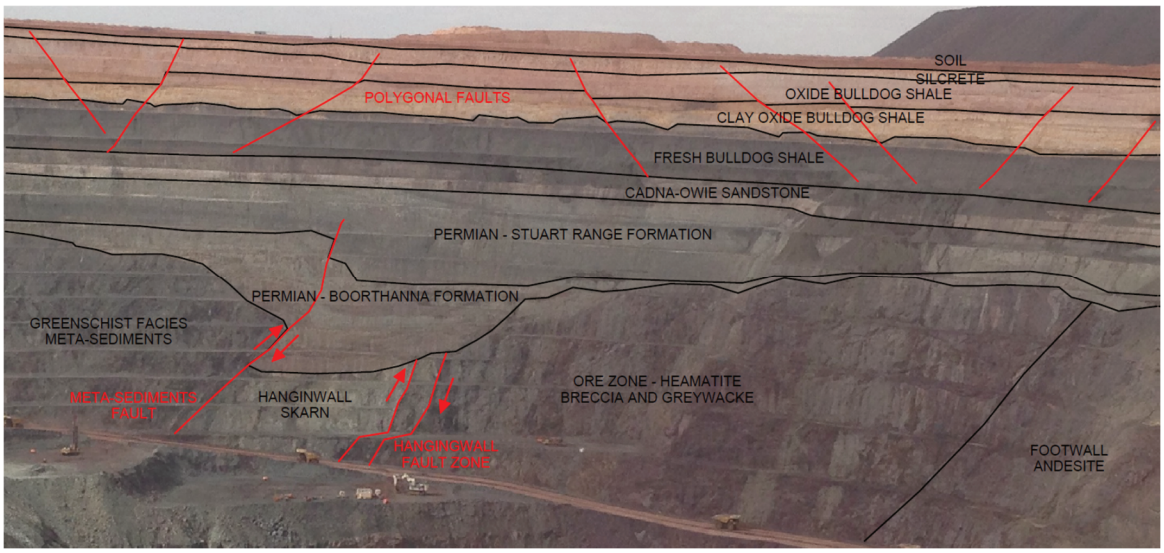


**Figure 7 Annotated photo of the east wall of the Prominent Hill open pit, showing both the cover sequence and basement rocks. Polygonal faults are the red lines in the upper part of the photo within the Bulldog Shale units**

## 3.2 Engineering properties of materials

Typical engineering properties based primarily on drillcore for all units are presented in Table 1. The overall rock mass conditions are somewhat inverted, where rock mass conditions decrease with depth until the Permian units are encountered. The silcrete presents as a medium strength, highly fractured rock. The oxidised Bulldog Shale is a low strength, bedded, and occasionally jointed weak rock unit. The fresh Bulldog Shale is a very low strength bedded unit and is highly expansive, and on exposure to the atmosphere swells breaking down to a soil. The Cadna-owie Sands are a variably cemented sand. The general rock mass condition improves significantly in the Permian sediments.

**Table 1 Summary of geotechnical characteristics – cover sequence**

| Geotechnical unit | Weathering | Rock quality designation (%) | Static durability (Dusseault et al. 1983) | Typical field estimated strength |
|---|---|---|---|---|
| Silcrete | Highly | 20–70 | NA | R3 |
| Bulldog Shale oxidised | Highly to moderately | 60–100 | No – high deterioration, typically medium | R2–R1 |
| Bulldog Shale fresh | Slightly | 70–100 | Medium – total deterioration, typically high | R1–R2 |
| Cadna-owie Sands | Slightly | Significant lengths of core loss and soil strength material | Medium – total deterioration (limited results) | Soil strength – R0 |
| Permian sediments | Slightly to fresh | 80–90 | Not tested | R2–R3 |

Limited unconfined compressive strength (UCS) and soil shear box testing was available as summarised in Tables 2 and 3.

**Table 2 Summary of UCS testing – cover sequence – all data**

| Geotechnical unit | Number of tests | Average UCS (MPa) | Maximum UCS (MPa) | Minimum UCS (MPa) |
|---|---|---|---|---|
| Silcrete | 2 | 8.1 | 12.9 | 3.2 |
| Oxidised Bulldog Shale | 8 | 3.7 | 8.9 | 0.2 |
| Fresh Bulldog Shale | 4 | 2.9 | 5.7 | 0.7 |
| Cadna-owie Sands | 1 | 1.9 | NA | NA |
| Permian sediments | 4 | 4.4 | 10.1 | 0.03 |

**Table 3 Soil shear box testing – cover sequence**

| Borehole | Depth (m) | Lithology | Peak cohesion (kPa) | Peak friction angle (°) |
|---|---|---|---|---|
| PH05D176 | 74.9 | Cadna-owie Sands | 0 | 38 |
| PH05D176 | 87.1 | Permian sediments | 100 | 36 |

### 3.2.1 *Atterberg limits of cover sequence rocks*

The results of Atterberg limits testing for cover sequence rocks are presented in Figure 8. The results indicate that:

- Remoulded oxidised Bulldog Shale behaves like high plasticity silt (MH).
- Remoulded fresh Bulldog Shale behaves like a high plasticity silt to clay (MH-CH).
- Remoulded plastic portions of the Cadna-owie Sands behave like medium to high plasticity clays (CI-CH).
- Permian sediments behave like medium to low plasticity clays (CI-CL).

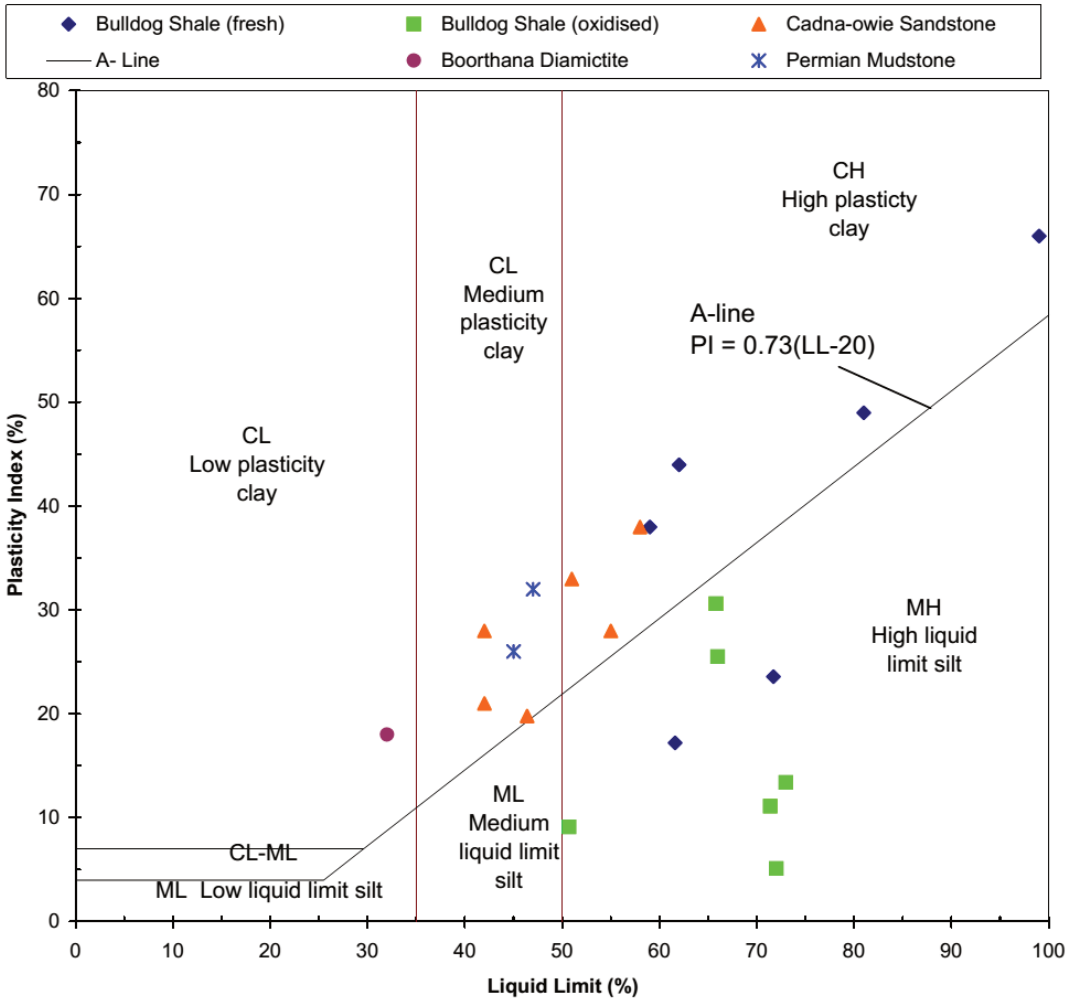


**Figure 8 Atterberg limits testing for cover sequence rocks**

### 3.2.2 *Clay mineralogy of the fresh Bulldog Shale*

A sample of fresh Bulldog Shale from a depth of 63 m was analysed using X-ray diffraction analysis (XRD). The results are summarised in Table 4. Significantly, the Bulldog Shale comprises a high percentage of the reactive mixed illite-smectite clays. Illite is typically moderately reactive whilst smecite can be moderately to highly reactive. Mineralogy suggested that the montmorillonite (another term for smectite) is most likely to be magnesium rich rather than iron rich, which is in keeping with the interpretation that it is of marine origin.

**Table 4 XRD result of fresh Bulldog Shale**

| Phase | Weight (%) | Error (%) |
|---|---|---|
| Quartz | 20.1 | 1.21 |
| Illite | 13.3 | 1.94 |
| Kaolinite | 8.9 | 1.62 |
| Anorthite | 5.9 | 1.58 |
| Pyrite | 0.3 | 0.27 |
| Mixed layer illite-smectite | 51.6 | 2.74 |

A sample of fault gouge taken from a pit exposure presented in Table 5 produced similar, albeit slightly higher, montmorillonite results. Whilst mineralogy is not directly related to strength, common correlations suggest effective shear strengths in the order of 13–15°.

**Table 5 XRD result of fault gouge in fresh Bulldog Shale**

| Phase | Weight (%) | Error (%) |
|---|---|---|
| Quartz | 11.7 | 0.61 |
| Montmorillonite | 62.2 | 0.65 |
| Barite | 22.0 | 0.30 |
| Kaolinite | 4.1 | 0.69 |

### *3.2.3 Triaxial testing of fresh Bulldog Shale*

Multistage consolidated undrained triaxial testing with pore pressure measurements was undertaken on the Bulldog Shales. Figure 9 presents the p'-q plot of all samples throughout the sequence, noting that the lower layers in the sequence are the weaker of the samples. The p'-q plot is presented using the Massachusetts Institute of Technology (MIT) methodology, with both peak and residual test results presented. Overall peak effective shear strengths are assessed to be c' = 250 kPa, phi' = 20° and residual effective shear strengths c' = 0 kPa, phi' = 20°.

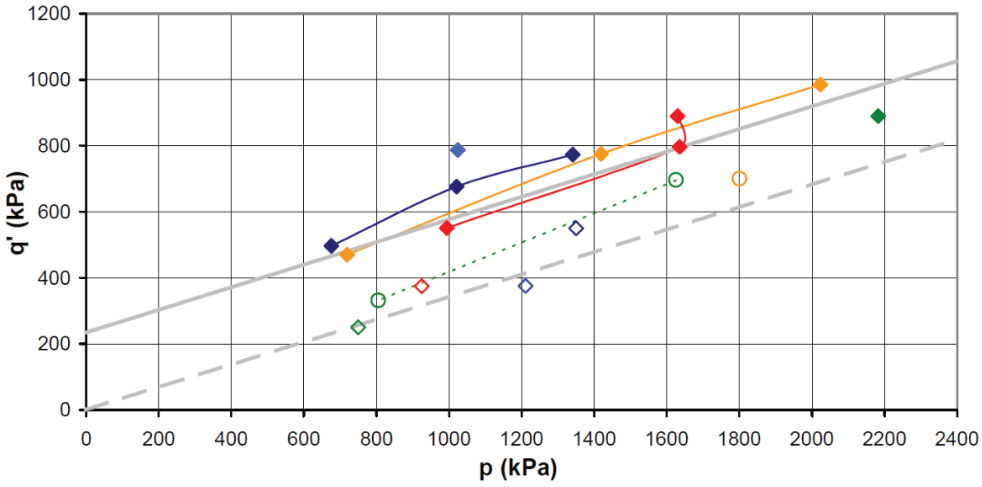


**Figure 9 MIT p'-q plot of triaxial strength of fresh Bulldog Shale. Solid and closed symbols represent peak and residual stages respectively. The solid grey line represents a visual fit for peak effective shear strengths at c' = 250 kPa, phi' = 20° and the dashed grey line, a visual fit for residual strengths at c' = 0 kPa, phi' = 20°**

## 3.3 Structure

Primary structure in the cover sequence comprises largely horizontal bedding with the exception of areas affected by faults and in Permian units which are draped over the irregular basal unconformity with the underlying basement rocks. Some short (typically < 2 m) sub-vertical jointing exists particularly in the silcrete and weathered Bulldog Shale as shown in Figures 10a and 10b.

(a) (b)

**Figure 10 (a) Silcrete showing closely spaced defects resulting in blocky rock mass conditions; (b) Showing jointed weathered Bulldog Shale**

Faulting is the most geotechnically significant defect in the cover sequence. The faults are relatively thin, typically only 10 mm thick with little to no damage around the plane as shown in Figures 11a and 11b. Offsets are common and are typically only metres of dip displacement. Weathering is often deeper around faults. Fault surfaces terminate toward the contact with the Cadna-owie Sand.

The orientation of discontinuities from mapping of pit exposures is summarised in Figure 12. The orientation of faults (red and orange symbols) dip at approximately 60° with a dispersed dip direction. This is consistent with both the theory and example of polygonal mapping from Lake Hope (Cartwright & Dewhurst 1998; Watterson et al. 2000). Notwithstanding this consistency, no direct observation of polygonal cells has been observed in exposures.

(a) (b)

**Figure 11 (a) A polygonal fault plane in the transition from the weathered to fresh Bulldog Shale; (b) A close-up of the fault and slickensided nature of the contact plane in the Bulldog Shale, showing the polished surfaces**

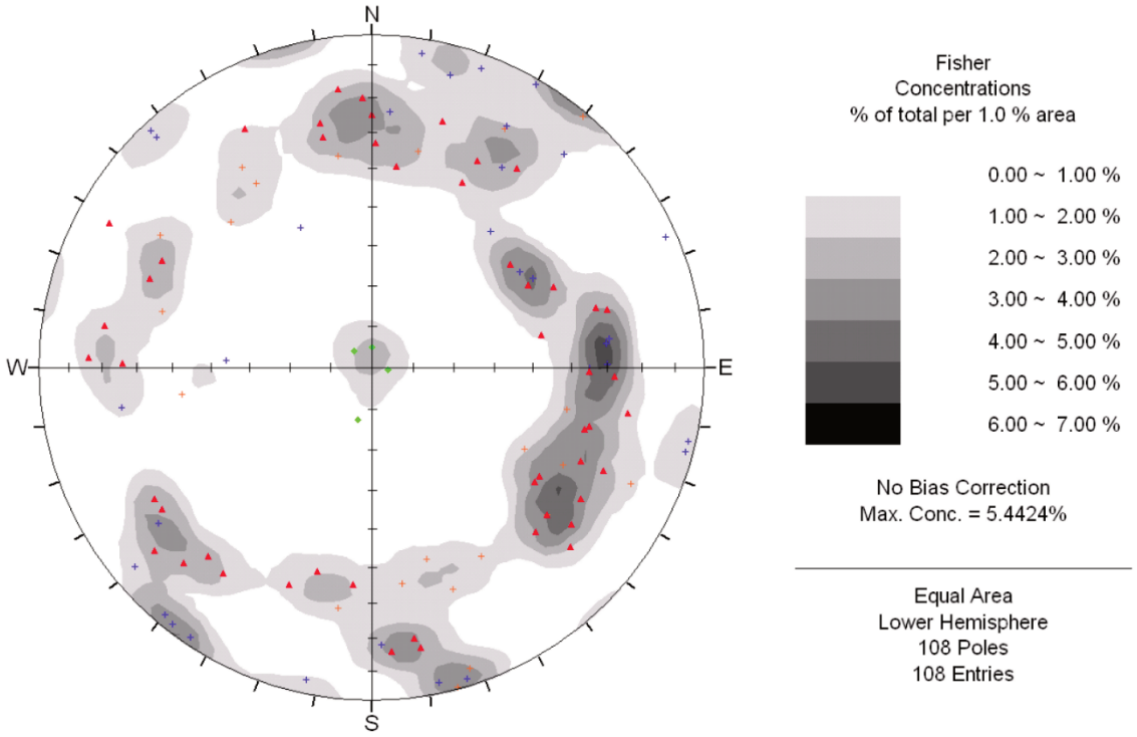


**Figure 12 Stereographic projection of mapped discontinuities. Red and orange symbols represent faults, blue symbols represent joints, and green symbols represent bedding**

The spatial distribution of faults varies around the pit as shown in Figure 13. Faults are typically spaced between 50–250 m apart. In some locations, two faults of opposing orientations in close proximity create small grabens.

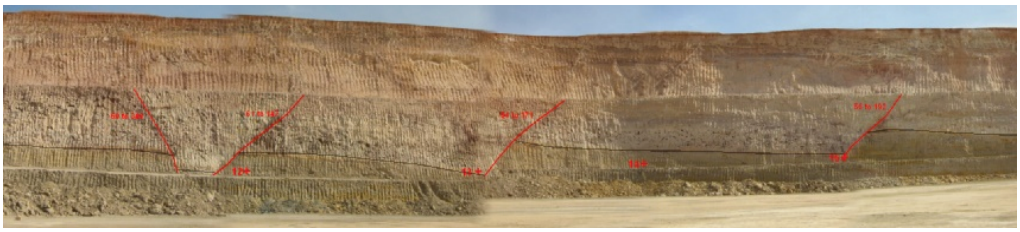

**Figure 13 Photomontage showing the spatial distribution of faults (red) and bedding (black) in the upper few benches in weathered Bulldog Shale. The approximate height of the slope is 40 m**

## 3.4 Hydrogeology

The pore pressure condition at Prominent Hill is complex and is not fully addressed in detail in this paper. For reference, the permeability of the fresh Bulldog Shale was estimated to be 5–11 m/s. Groundwater monitoring of the cover sequence comprised both vibrating wire piezometers (VWP) and conventional standpipe piezometers around the perimeter of the pit. A number of trends are observed from piezometers:

- Grouted-in-place vibrating wire sensors installed in the fresh Bulldog Shale took up to two months to equilibrate, suggesting very low permeability.
- Stabilised piezometers the Bulldog Shale measured various levels of head above the base of the Bulldog Shale.
- Those piezometers located in the Cadna-owie Sand read zero pressure, indicating that this unit was drained.
- Piezometric measurements in the basement rocks indicate hydrostatic conditions with heads lower than the contact with the overlying sediments.

Figure 14 is a summary of pore pressures measured from VWPs and standpipes, and presents pressure head versus elevation of sensor or screened interval.

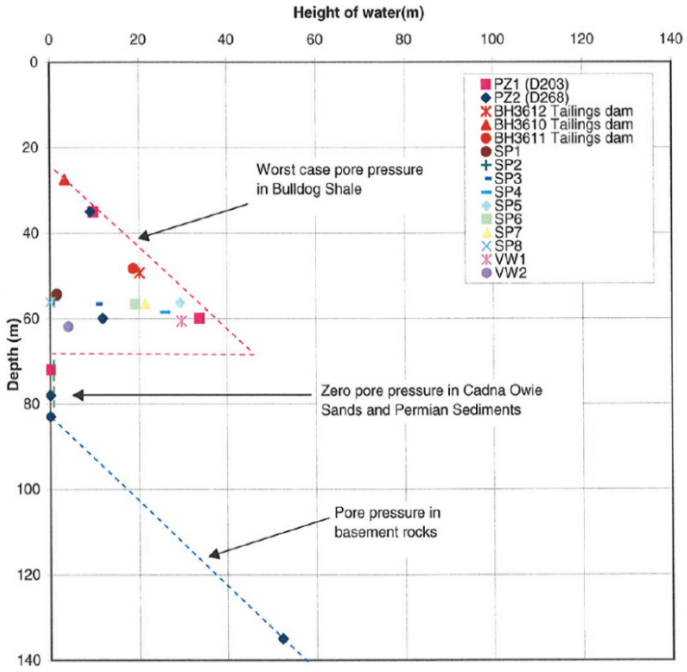


**Figure 14 Depth versus pressure heads for equilibrated contemporaneous piezometer measurements**

The pore pressures in the Bulldog Shale are interpreted to be perched water which is consistent with its very low permeability. The variability of pressures in the Bulldog Shale is possibly related to proximity to underdrainage caused by the highly permeable Cadna-owie Sand. Variability is also thought to be related to proximity to polygonal faulting which are likely drainage paths to the Cadna-owie Sand. There is an interval of lower cover sequence below the Cadna-owie Sand and the upper basement which is drained. The basement appears hydrostatic below this.

The strategy for latter stages of mining-included groundwater interception wells in the cover sequence and long horizontal drain holes which targeted polygonal faulting in the Bulldog Shale. These efforts were effective in reducing pore pressure and improving stability but are not presented here.

# 4 Design approach

## 4.1 Failure mechanisms

The understanding of failure mechanisms evolved during the investigation and mining stages of the project. The following section provides an overview of mechanisms sufficient to describe analytical techniques. Additional detail is provided in Section 5 which describes slope performance and actual failures. Three mechanisms have been used to assess stability as outlined below:

- Conventional circular failure, which was not considered critical but undertaken as a check.
- Planar block sliding, bound by a fault at the rear and horizontal sliding on the base in the lower fresh Bulldog Shale. Sliding on the base requires consideration of strength anisotropy parallel to bedding.
- Non-daylighting wedge bound by two faults with sliding on the bedding in the lower fresh Bulldog Shale. Anisotropic strengths were also employed here.

The latter two mechanisms are similar and are considered to the most representative. All three mechanisms are sensitive to pore pressure.

## 4.2 Parameters

The strength parameters used for the design of slopes at the Prominent Hill mine have evolved and been updated as new data from both testing and back-analysis of failures have occurred. The following design parameters are the most up to date.

Table 6 presents the densities and Mohr–Coulomb effective strength parameters used in limit equilibrium stability analysis. It is of note that initially the silcrete layer and oxidised Bulldog Shale were modelled with a tension crack enabled. The fresh Bulldog Shale parameters are similar but not the same to those presented in Section 3.2.3 owing to feedback from back-analysis.

**Table 6 Cover sequence model parameters**

| Geotechnical unit | Strength parameters | | |
|---|---|---|---|
| | Density (kN/m$^3$) | Cohesion (kPa) | Friction angle (°) |
| Silcrete[1] | 19 | 1,160 | 43 |
| Oxidised Bulldog Shale[1] | 17 | 450 | 36 |
| Clay Oxidised Bulldog Shale | 17 | 100 | 33 |
| Fresh Bulldog Shale[2] | 18 | 40 | 20 |
| Cadna-owie Sands | 17 | 20 | 35 |
| Permian sediments | 23 | 260 | 35 |

[1]With tension crack enabled. [2]Parallel to bedding based on back-analysis.

Modelling was undertaken considering the following additional detail:

- Fresh Bulldog Shale strengths presented were for use on block sliding mechanisms where the failure plane is parallel to bedding.
- Fault strengths were assumed to be cohesionless; phi' = 15° or 20°. The upper strength was based on the residual strength from triaxial testing presented in Section 3.2.3. However, this appeared high compared with expectations from mineralogy and Atterberg limits, so analyses were also undertaken using the lower strength.
- Pore pressure profile was assumed as shown in Figure 14 (pink dashed line). Both hydraulic coefficient Hu = 1 and Hu = 0.7 were used to account for the variability in pressure.

## 4.3 Design methodology

The analytical approach to cover sequence slopes design comprised:

- Two-dimensional limit equilibrium circular assessment of mass properties.
- Two-dimensional limit equilibrium block path modelling of fault at the rear with sliding on bedding the base (Figure 15).
- Two-dimensional limit equilibrium composite circular failure through the rear of the slide with sliding on bedding the base.
- Two-dimensional finite element modelling to confirm mechanisms and estimates of Factor of Safety.
- Three-dimensional rigid block analysis.

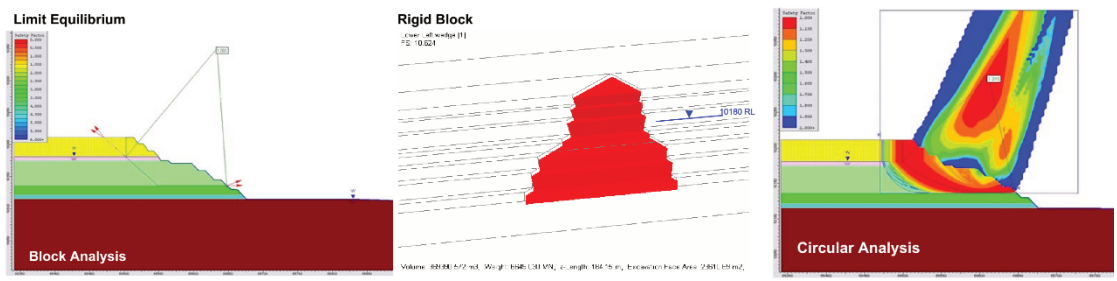


**Figure 15 Examples of analyses undertaken for stability of slopes in the cover sequence. The left figure is 2D limit equilibrium block path modelling of fault at the rear with sliding on bedding, central figure is the rigid block 3D analysis, right is 2D limit equilibrium circular failure through the rear of the slide with sliding on bedding at the base**

Sensitivities were undertaken on:

- Pore pressure.
- Fault strength.
- Fault dip.
- Fault location with respect to the toe.

A semi-probabilistic approach was used to assess the fault dip and proximity to the face as a means of predicting the likelihood of failure.

# 5 Slope design and performance

## 5.1 Slope design

Slope designs of the cover sequence at Prominent Hill evolved throughout the project as both the knowledge of the ground conditions and project risk tolerance evolved. Initial inter-ramp slope angles in the cover sequence were 38° and performed adequately in the absence of polygonal faulting; however, large zones where faulting occurred failed following excavation. Slope angles have progressively reduced throughout scheduled stages and are now 26° and slightly flatter in some critical locations. Notwithstanding the significant reduction in slope angles, large failures still occur, albeit at reduced frequency and with reduced runout.

## 5.2 Slope performance

As described previously, large parts of the cover sequence slopes failed. Figure 16 presents a plan showing the stage 2 pit slope indicating the zones that have failed or are moving. The stage 2 inter-ramp slope angle in the cover sequence was 34°. The area of failure as a percentage of the total wall exposed (not including areas flattened by ramps) is approximately 20%, and a further 25% of the slopes were experiencing movement.

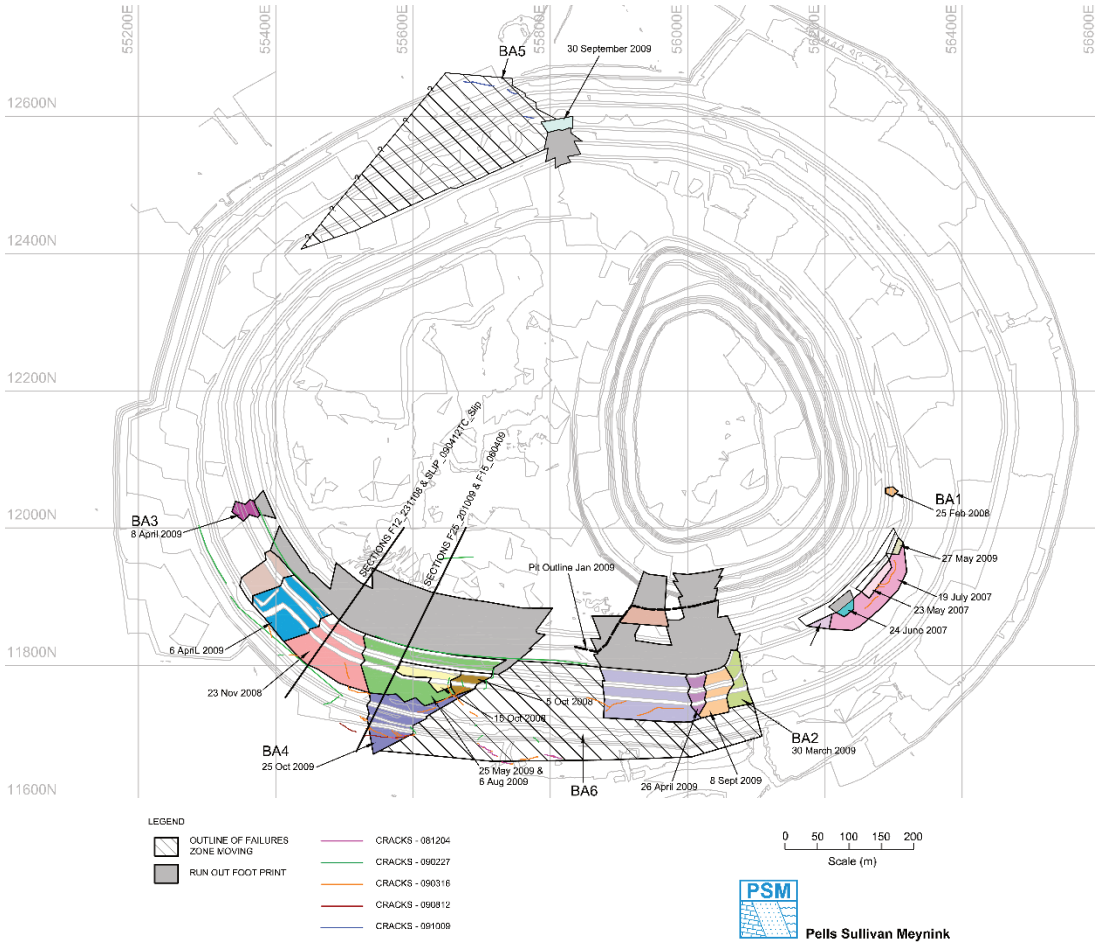


**Figure 16 Stage 2 Pit showing the areal extent of failures or zones undergoing significant movement**

## 5.3 Failure examples

Examples of failures observed are presented in Figures 17 to 20 and cover the spectrum of scales. The examples are taken from different mining stages. A discussion of the common features of failures is presented thereafter.

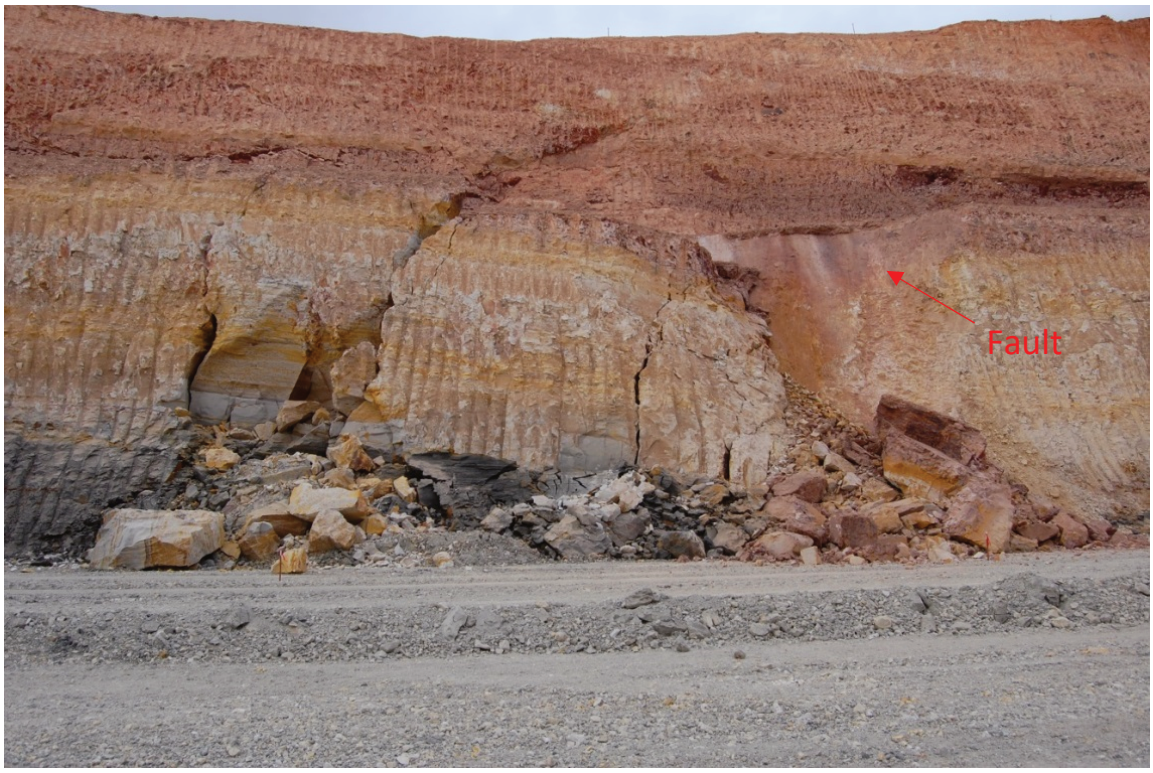


**Figure 17** **Small one-sided wedge, fault-bound on one side with failure through rock mass on the other. This is one bench high (15 m)**

**Figure 18** **Small non-daylighting wedge, where two faults define a block with a hinge line that is steeper than the slope angles. Failure develops by sliding on bedding at the base. This is two benches high (30 m)**

**Figure 19 Medium-sized failure showing runout over the working surface. This is about 50 m high**

**Figure 20 Larger-scale (>200,000 BCM) non-daylighting wedge over the inter-ramp scale with significant runout over the working floor**

## 5.4 Common factors of failures and proposed failure mechanisms

A summary of the common features of failures is set out below and a conceptual failure mechanism is presented in Figure 21:

1. Initial failures have been exclusively bounded at the rear by moderately dipping faults (polygonal origin):
    - Either formed as a wedge where two faults intersect; or
    - One fault with failure through the rock mass on the other side; or
    - One fault only.
2. Most commonly, the inter-ramp angle is shallower than the hinge line of the wedge or planar failure; that is the structures do not daylight.
3. Sliding at the base occurs along horizontal bedding planes to produce what is termed a 'block sliding' type of mechanism. The block is, however, not rigid.
4. Seepage is often seen emanating from at or near the basal failure plane.
5. Lipping commonly occurs at or near the contact between the Bulldog Shale and the Cadna-owie Sands.
6. All failures are above the Cadna-owie Sands.
7. Tension cracking occurs in the silcrete and oxidised Bulldog Shale some distance inside the projected fault intersection at the surface. Cracking generally develops when excavation reaches midway down through the fresh Bulldog Shale.
8. Prism monitoring indicates relatively small deformation immediately following full excavation of the cover sequence. At this point, the difference is not readily discernible between a slope that will continue to move to failure and one that will eventually stabilise. Over the following one to many months, displacements for those slopes which fail, accelerate and eventually collapse.
9. It is common for precursor smaller failures to develop along the toe or on leading edges before large blocks fail. The effect of these smaller failures is reflected in slight increases in rates of movement in the prism displacement graphs.
10. Rainfall is very limited at Prominent Hill with an annual rainfall of approximately 100–200 mm per year. The link between rainfall and the size and number of failures shows little correlation. Rainfall events do cause a slight increase in acceleration in already mobile slopes.
11. There appears to be no link between blasting and movements.
12. There appears to be very little evidence of additional impact due to the excavation of the basement materials.
13. Runout distances of materials after failure can be quite large. The controls on runout are the mechanical properties of the material and the height above the floor of the failure mass.
14. The scale of failures ranges from less than bench-scale up to around 200,000 $m^3$.

Figure 21 shows notional pore pressures acting on the base of the block along bedding and at the rear of the block within the polygonal fault. Pore pressures are discussed further in the following section.

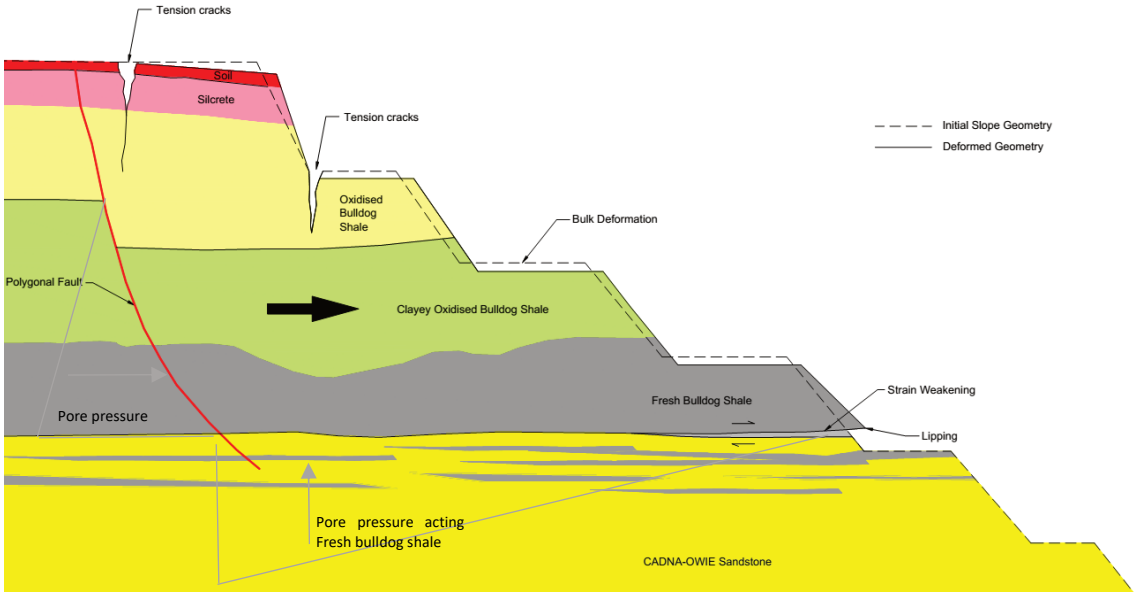


**Figure 21 Conceptual failure mechanism**

## 5.5 Delayed onset of collapse

One of the notable features of these failures is the delay between daylighting the base of the Bulldog Shale (and the toe of most failures) and the onset of collapse. This is demonstrated in Figure 22 where modelled displacements presented in the upper plot are compared with equivalent prism measurements from an actual failure. In the upper plot, displacements occur on daylighting the fresh Bulldog Shale. Whereas in reality, the collapse occurred some 12 months after the fresh Bulldog Shale was daylighted. The aqua coloured prism (10175 37) that reached failure before the failure of the overall mass was related to a subsidiary event.

Almost all failures involving sliding on bedding in the fresh Bulldog Shale exhibited a delay between excavation of the toe of the ultimate failure surface and collapse of the slope. The magnitude of the delay was somewhat dependant on the size of the failure and ranged from one month for single bench failure to one year for full cover sequence failures.

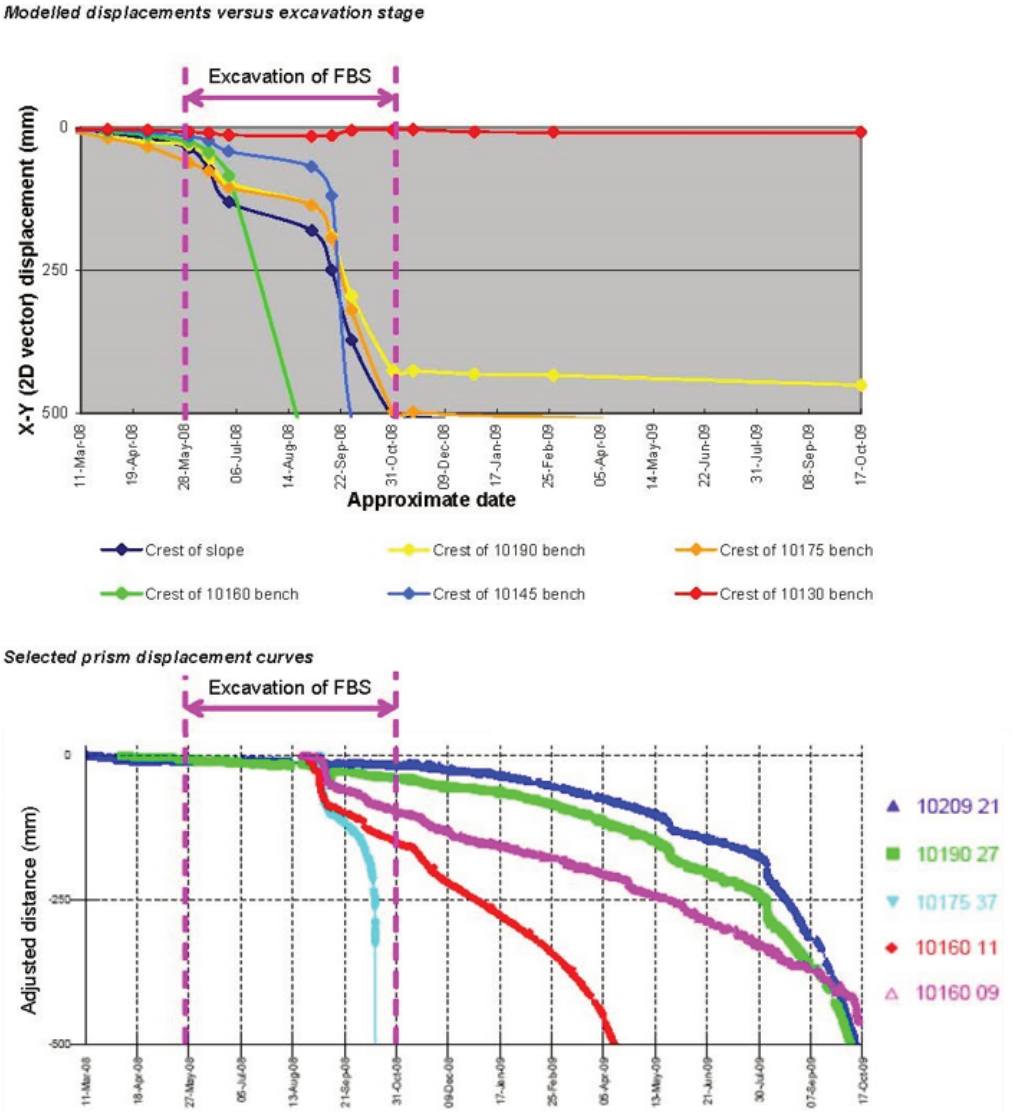


**Figure 22 Modelled (upper) and measured (lower) slope deformation of a large failure at Prominent Hill highlighting delayed collapse of the slope**

The most likely causes of the delay were strain weakening and hydromechanical coupling as listed below:

- The strain weakening effect is the reduction in the strength of material to residual shear strength after movement past peak shear strength as discussed in Section 5.3.1.2 of Martin & Stacey (2018). In its simplest form, this effect was demonstrated in the laboratory during triaxial testing where peak strengths drop to residual strengths, although the reduction in strength was small. Further, the loading case at slope scale is more complex than laboratory-scale tests. For example, the load comes onto different beds in the Bulldog Shale at different times as the excavation develops.
- Here, hydromechanical coupling is caused by unloading of the slope. Pore pressure response to unloading was first documented by Bishop & Bjerrum (1960) as shown in Figure 23. In this hypothetical example, a slope is unloaded by rapid excavation. Unloading causes initial negative pore pressures to develop, resulting in a temporary improvement in stability. Over time, the pore pressures rebound and stabilise, reducing stability. Hydromechanical coupling at the scale of mine slopes is of course more complex than this and is documented by Sullivan (2007) and more recently Sullivan (2020). The hydromechanical coupling experienced as part of the block sliding mechanism (described in Section 5.4) is complex because unloading occurs progressively. The unloading effect is interpreted to have the greatest effect along the base of the block where the shear plane

develops parallel to bedding fabric through intact material with very low permeability and less so in the polygonal fault with higher permeability.

- In the authors' view, hydromechanical coupling is considered the primary reason for the long delay in onset of collapse.

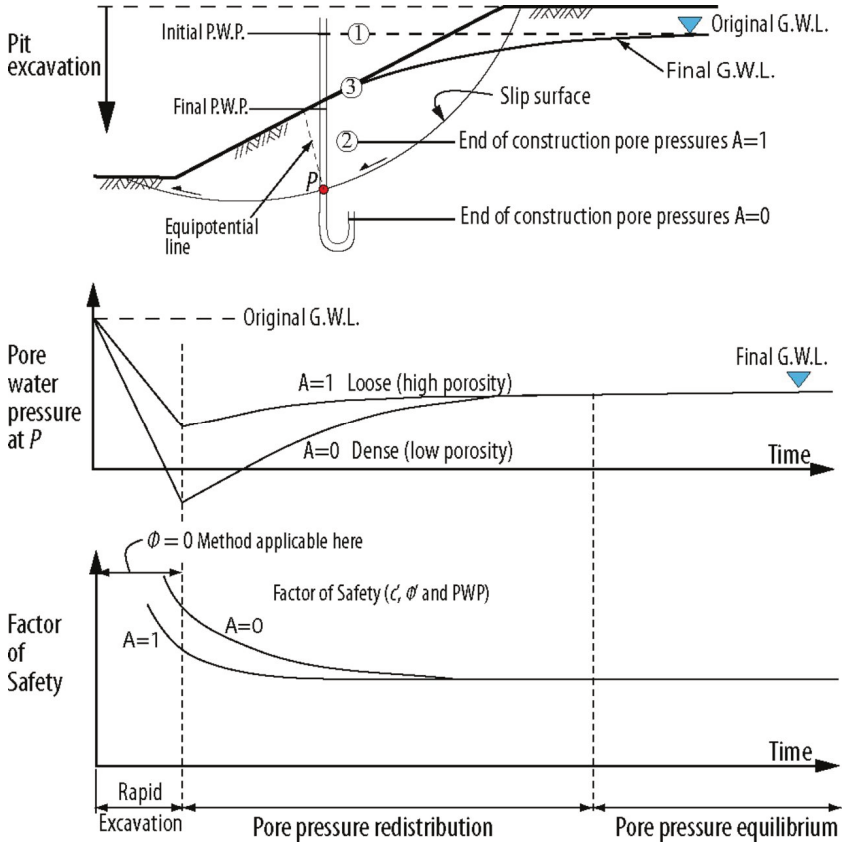


**Figure 23 Variation in Factor of Safety with time for an excavation of a slope (after Bishop & Bjerrum 1960)**

## 5.6 Runout distance

The runout distance of failures affects the risk to operations and clean-up effort required. The runout distance for four failures is presented in Figure 24 showing pre-failure and post-failure surface and the runout geometries. In summary the data indicates:

- The runout distance ranges from 20–150 m; greater distances would be expected if the working floor were deeper.
- The length of runout is affected by both the height of the failure and height of the failure above the mining bench.
- The runout slope angles range from 14–36°, although site personnel give another example where this angle is 12°.

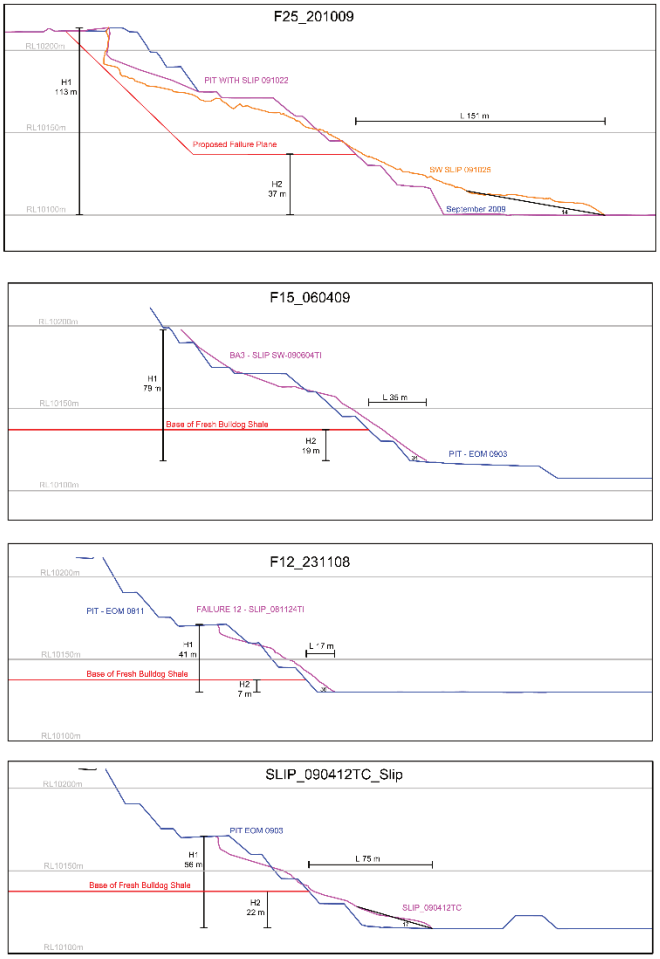


**Figure 24 Cross-section through four failures showing the pre-failure and post-failure geometries**

## 5.7 Back-analysis

The performance of slopes have been the subject of ongoing review and analysis. Failures were back-analysed in campaigns and presented in a systematic way as shown in Figure 25. This systematic presentation aided ease of comparison and consistent analytical approach. Back-analysis comprised parametric analysis utilising two-dimensional and three-dimensional approaches. Strengths derived from this process were used in forward predictions.

One of the learnings during analysis was that it was critical to carry the same assumptions into the forward-analyses as those assumed in the back-analysis. Departure from the assumptions, for example, using a pore pressure grid instead of a simple groundwater surface with hydraulic parameter Hu, or omitting tension cracking, had a very significant artificial impact on results.

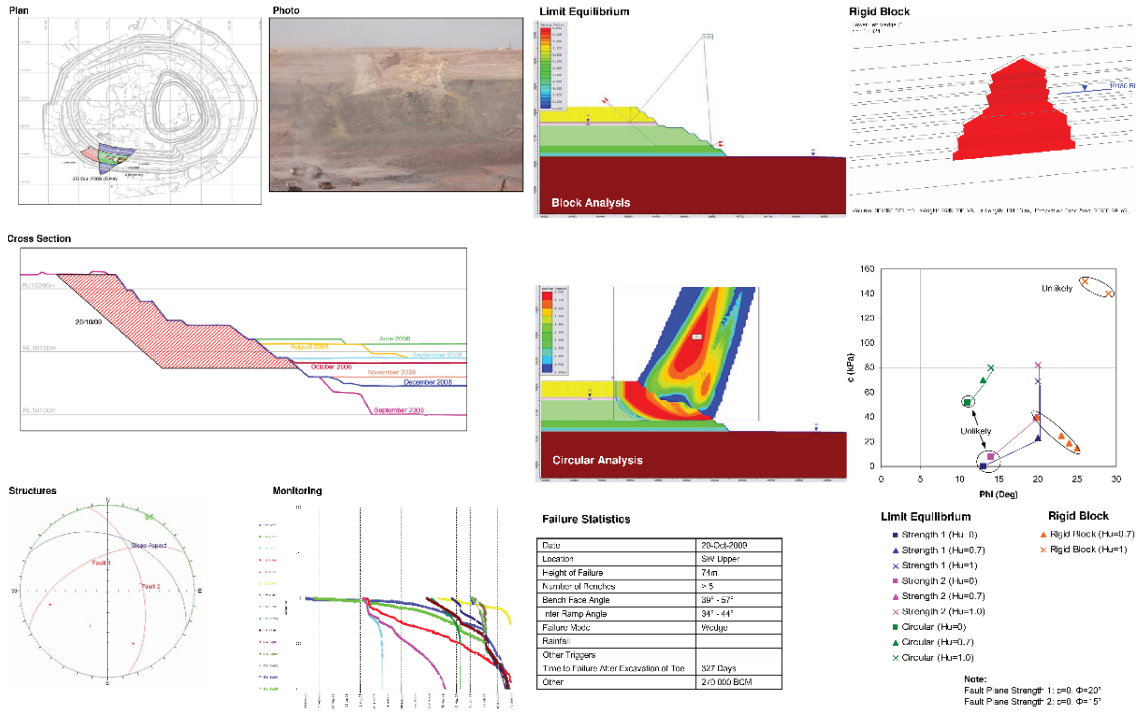


| Failure Statistics | |
|---|---|
| Date | 20-Oct-2009 |
| Location | SW Upper |
| Height of Failure | 74m |
| Number of Benches | > 5 |
| Bench Face Angle | 35° - 57° |
| nter Ramp Angle | 34° - 44° |
| Failure Mode | Wedge |
| Rainfall | |
| Other Triggers | |
| Time to Failure After Excavation of Toe | 327 Days |
| Other | 2x0 000 BCM |

**Figure 25 Example of systematic presentation of failure back-analysis**

# 6 Discussion

The initial slope performance of cover sequence rock at Prominent Hill was outside of the range of expected behaviour. A significant amount of work was undertaken to understand the ground conditions and their relationship to stability.

The occurrence of unfavourable faulting was the key driver for instability. The block sliding failure mechanism meant that stability was somewhat insensitive to overall slope angle. This was because reducing the overall slope angle reduced both the driving and resisting components of the slide. So, while revision to the geometry and reduction in inter-ramp slope angle was chosen, the outcome was a reduced frequency but not elimination of slope failure. Further flattening came at considerable economic penalty and so a higher than normal extent of slope failures was accepted.

Mining schedules included allowances for four million bulk cubic metres for unloading and clean-up as required such that additional failures could be treated on an as-needed basis.

The ground control management plan including trigger action response plans (TARPs), based around the use of robotic survey prism and radar monitoring, were adequate for controlling hazards associated with instabilities. The development of procedures was assisted by the recurrence of failures. The delayed onset of collapse provided adequate time to plan and execute remediation and clean-up.

# 7 Conclusion

The combination of weak anisotropic substance strength, polygonal faulting and high pore pressures resulted in challenging operational conditions in the weak sedimentary rocks of the cover sequence at Prominent Hill. The occurrence of polygonal faulting had the largest stability impact. The delayed onset of collapse is caused by both strain softening and hydromechanical coupling, with the latter being considered the dominant of the two.

Key features about the slope performance include:

- Slope angles were reduced from initial designs, although extensive failures still occurred.
- Further flattening came at considerable economic penalty, and so a higher than normal extent of slope failures was accepted.

  This was somewhat offset by:

- The delayed onset of collapse of slopes which, in some instances, took up to a year to manifest. The delay meant that there was adequate time to put in place controls and adjust mining schedules.
- Sound pit slope management processes and monitoring which included both prism surveying and slope radar monitoring.

## Acknowledgement

The authors thank OZ Minerals Ltd for permission to publish the paper and the OZ Minerals Ltd geotechnical department including Tom Liubinas, James Marker, Rhys Harris and Nathalia Revelo-Mendez.

## References

Bishop, AW & Bjerrum, L 1960, *The Relevance of Triaxial Test to the Solution of Stability Problems*, Publication No. 34, Norwegian Geotechnical Institute, Oslo.

Cartwright, JA & Dewhurst, DN 1998, 'Layer-bound compaction faults in fine-grained sediments', *GSA Bulletin*, vol. 110, no. 10, pp. 1242–1257.

Duran, A 2014, 'Comparison of field estimated strengths', *Proceedings of AUSROCK 2014: Third Australasian Ground Control in Mining Conference*, The Australasian Institute of Mining and Metallurgy, Melbourne, pp. 101–106.

Dusseault, M, Cimolini, PH, Soderberg, H & Scafe, D 1983, 'Rapid index tests for transitional materials', *Geotechnical Testing Journal*, vol. 6, no. 2, pp. 64–72.

Geological Survey of South Australia 1993, *The Geology of South Australia*, Geological Survey of South Australia, Adelaide.

Martin, D & Stacey, P 2018, *Guidelines for Open Pit Slope Design in Weak Rocks*, CSIRO Publishing, Clayton.

OZ Minerals Ltd 2009, *OZ Minerals Sustainability Report 2009*, OZ Minerals Ltd, Adelaide, viewed 6 September 2021, https://www.ozminerals.com/uploads/media/OZM_sustainability09_web-be7621cf-090c-4948-b831-2dce20cfec24-0.pdf

Sullivan, TD 2007, 'Hydromechanical coupling and pit slope movements', in Y Potvin (ed.), *Slope Stability 2007: Proceedings of the 2007 International Symposium on Rock Slope Stability in Open Pit Mining and Civil Engineering*, Australian Centre for Geomechanics, Perth, pp. 3–43, https://doi.org/10.36487/ACG_repo/708_Sullivan

Sullivan, TD 2020, 'Hydromechanical coupling concepts for mine slopes', in PM Dight (ed.), *Slope Stability 2020: Proceedings of the 2020 International Symposium on Slope Stability in Open Pit Mining and Civil Engineering*, Australian Centre for Geomechanics, Perth, pp. 66–98, https://doi.org/10.36487/ACG_repo/2025_0.04

Watterson, J, Walsh, J, Nicol, A, Nell, PAR & Bretan, PG 2000, 'Geometry and origin of a polygonal fault system', *Journal of the Geological Society*, vol. 157, no. 1, pp. 151–162.